# Sulfur-impurity induced amorphization of nickel

Zaoshi Yuan, Hsiu-Pin Chen, Weiqiang Wang, Ken-ichi Nomura, Rajiv K. Kalia, Aiichiro Nakano,[a] and Priya Vashishta

*Collaboratory for Advanced Computing and Simulations, Department of Chemical Engineering and Materials Science, Department of Physics and Astronomy, and Department of Computer Science, University of Southern California, Los Angeles, California 90089-0242, USA*

(Received 10 May 2011; accepted 5 August 2011; published online 16 September 2011)

Recent experimental and theoretical studies have shown an essential role of sulfur segregation-induced amorphization of crystalline nickel leading to its embrittlement at a critical sulfur concentration of ~14%, but the atomistic mechanism of the amorphization remains unexplained. Here, molecular dynamics simulations reveal that the large steric size of sulfur impurity causes strong sulfur-sulfur interaction mediated by lattice distortion up to the next nearest-neighbor lattice sites and that amorphization occurs at the percolation threshold of the sulfur-sulfur network with the next nearest-neighbor connectivity. Furthermore, the generality of the amorphization mechanism due to the percolation of an impurity network is confirmed for a model binary material. © *2011 American Institute of Physics*. [doi:10.1063/1.3636368]

## I. INTRODUCTION

The unusual mechanical behavior of nanocrystalline materials has been studied extensively, where the greatly increased ductility or dramatically enhanced strength and hardness are thought to arise from intricate interplay among dislocations, grain boundaries (GBs), and free surfaces within a relatively small volume.[1–5] However, alteration of the chemical composition at GBs by segregation of a small amount of impurities could cause intergranular brittleness of normally ductile nanocrystalline materials, thereby degrading their mechanical properties.[6–9] A prime example of such GB mechanochemistry[10] is sulfur (S) segregation-induced embrittlement of nickel (Ni) crystal.[11,12]

Fundamental understanding and control of embrittlement mechanisms in the Ni-S system are important not only scientifically but also technologically, e.g., for the development of next-generation nuclear reactors.[13] Experiments by Heuer *et al.*[12] showed that the critical S concentration of $15.5 \pm 3.4\%$ found for embrittlement is close to another critical S concentration, $14.2 \pm 3.3\%$, for amorphization of Ni during S ion implantation.[12] The experimentally found relation between GB embrittlement and amorphization was explained by a recent molecular-dynamics (MD) simulation involving $48 \times 10^6$ atoms[14] based on reactive force fields (ReaxFF).[15,16] Namely, an order-of-magnitude reduction of the GB shear strength due to amorphization, combined with tensile-strength reduction, provides an easy cleavage path at the crack tip.[14] This amorphization-induced embrittlement mechanism also explains an experimentally observed crossover from transgranular to intergranular fracture as well as suppression of plastic activities.[12]

Though the relation between S segregation-induced amorphization and embrittlement in Ni has thus been clarified, it remains unexplained why and how the sharp amorphization transition occurs within a narrow concentration range at the critical S concentration of ~14.2%. In this paper, we perform ReaxFF-MD simulations to study the change of structural properties of crystalline Ni as a function of S-impurity concentration. The simulation results reveal that the large steric size of S impurity causes strong S-S interaction mediated by the distortion of Ni crystalline lattice up to the next nearest-neighbor lattice sites and that amorphization occurs at the percolation threshold of the S-S network with the next nearest-neighbor connectivity. Furthermore, we confirm the generality of the amorphization mechanism due to the percolation of an impurity network for a model binary material described by the Lennard-Jones interatomic potential. This paper thus provides an atomistic mechanism of impurity-induced amorphization.

## II. STRUCTURAL AND THERMODYNAMIC PROPERTIES

MD simulations of S-doped Ni are performed using ReaxFF,[17] which significantly reduces the computational cost of simulating chemical reactions compared with quantum-mechanical (QM) calculations in the framework of density functional theory (DFT).[18,19] ReaxFF includes both bonded and nonbonded interactions. For bonded interactions, a general relationship between the bond length and bond order is used to obtain a smooth transition between different types of bonds and dissociation of bonds. In the force field, valence and torsion angles are formulated in terms of the bond order to ensure a continuous energy distribution upon dissociation of bonds during reactions. For nonbonded interactions, ReaxFF includes shielded van der Waals and Coulomb interactions. The total energy $E$ of the system is composed of various partial energy contributions:

$$E = E_{\text{bond}} + E_{\text{lp}} + E_{\text{over}} + E_{\text{under}} + E_{\text{val}} + E_{\text{pen}} + E_{\text{coa}} + E_{\text{tors}} + E_{\text{conj}} + E_{h\text{bond}} + E_{\text{vdWaals}} + E_{\text{Coulomb}}, \quad (1)$$

where $E_{\text{bond}}$ is the bond energy, $E_{\text{lp}}$ is the lone pair energy, $E_{\text{over}}$ and $E_{\text{under}}$ denote the over- and under-coordination

[a]Electronic mail: anakano@usc.edu.

 

energy, $E_{val}$ is the valence angle energy, a penalty function is included in $E_{pen}$, $E_{coa}$ describes the three-body conjugation energy, the torsion angle energy is $E_{tors}$, the four-body conjugation energy is $E_{conj}$, and the hydrogen bond interaction energy is included in $E_{hbond}$. In Eq. (1), nonbonded van der Waals and Coulomb interactions are described, respectively, by $E_{vdWaals}$ and $E_{Coulumb}$. The ReaxFF for Ni and S has been validated against experimental data and first-principles QM calculations based on DFT for the elastic constants and S impurity energies in Ni face centered cubic (fcc) crystal.[14]

ReaxFF-MD simulations are carried out to study S-induced amorphization of Ni. A set of cubic cells of size 35.2 Å containing 4000 atoms is used in this calculation, where periodic boundary conditions are applied in all three Cartesian directions. Ni atoms are randomly substituted by S atoms in the range of $8 \sim 18\%$.[12] For each S concentration, the system is relaxed by a steepest-descent procedure. Subsequently, the system is thermalized for 5 ps at 10 K and then gradually heated to 300 K.

To study the effect of S substitution on structural correlations, we calculate the pair distribution functions (PDF) $g(r)$ using the atomic coordinates from the MD simulations. Figure 1(a) shows the partial PDF, $g_{Ni\text{-}Ni}(r)$, between Ni atoms for three different S concentrations: $c_S = 8$, 14, and 18%. We observe that the peak heights in $g_{Ni\text{-}Ni}(r)$ decrease for increased S concentration, signifying increasing disorder. We also note that $g_{Ni\text{-}Ni}(r)$ at distance $r > 7$ Å has clearly separated peaks at $c_S = 8\%$, whereas they merge into broader features above $c_S = 14\%$, which indicates the disappearance of the longer-range structural order in Ni for $c_S > 14\%$.

To quantify the broadening of the peaks in PDF, we calculate the full width at half maximum (FWHM) of the first peak in $g_{Ni\text{-}Ni}(r)$ by Gaussian fitting, and plot it as a function of $c_S$ from 8 to 18% in Fig. 1(b). We see that the FWHM is well described by a linear function of $c_S$ before and after a critical concentration of ~14%, as shown by the linear fits of the FWHM versus $c_S$ by dash-dotted and dashed lines below and above 14%, respectively, in Fig. 1(b). The FWHM thus exhibits a discontinuity at $c_S \sim 14\%$.

Figure 1(c) plots the height of the second peak in $g_{Ni\text{-}Ni}(r)$ as a function of $c_S$. The behavior of the second-peak height changes dramatically before and after $c_S = 14\%$. Namely, it is a decreasing function of $c_S$ below 14%, while it takes a constant value for $c_S > 14\%$. These observations indicate sudden disordering of structure at a critical S concentration of ~14%, which agrees well with the experimental amorphization threshold of $14.2 \pm 3.3\%$.[12]

Besides the peak height in $g_{Ni\text{-}Ni}(r)$, the change in the bond length is also reflected by a shift of the first-peak position in $g_{Ni\text{-}Ni}(r)$ and a change in the coordination number at the first shell of neighbors. Namely, shorter Ni-Ni bonds are observed with increased S concentration, while the coordination number in Fig. 1(d) displays a small change from 11 to 9. The changes of the Ni coordination number and $g_{Ni\text{-}Ni}(r)$ may be attributed to the size effect.[20] The difference of the atomic radius between Ni and S drives the first and second peaks change systematically.[21] The larger S atoms tend to squeeze and push the surrounding Ni atoms, resulting in a decrease of the coordination number at the first nearest-neighbor distance.

The structural change as a function of S concentration is also manifested in bond angle distribution (BAD) as shown in Fig. 2(a), where the Ni-Ni-Ni BAD is plotted for $c_S = 8$, 14, and 18%. As $c_S$ increases from 14 to 18%, the position of the first peak at ~60° systematically shifts to a larger angle by three degrees as a result of decreasing coordination numbers, accompanied by dramatic broadening and decrease of its height. The structural disorder manifested as the broadening of BAD at $c_S = 18\%$ is comparable to that of amorphous Ni prepared by a melt-quench procedure as shown in Fig. 2(b), indicating a highly disordered structure.

To investigate the behavior of thermodynamic quantities of the Ni crystal induced by S impurities, we calculate the equilibrium volume of the system for different S concentrations. In Fig. 3, the solid circles represent the calculation

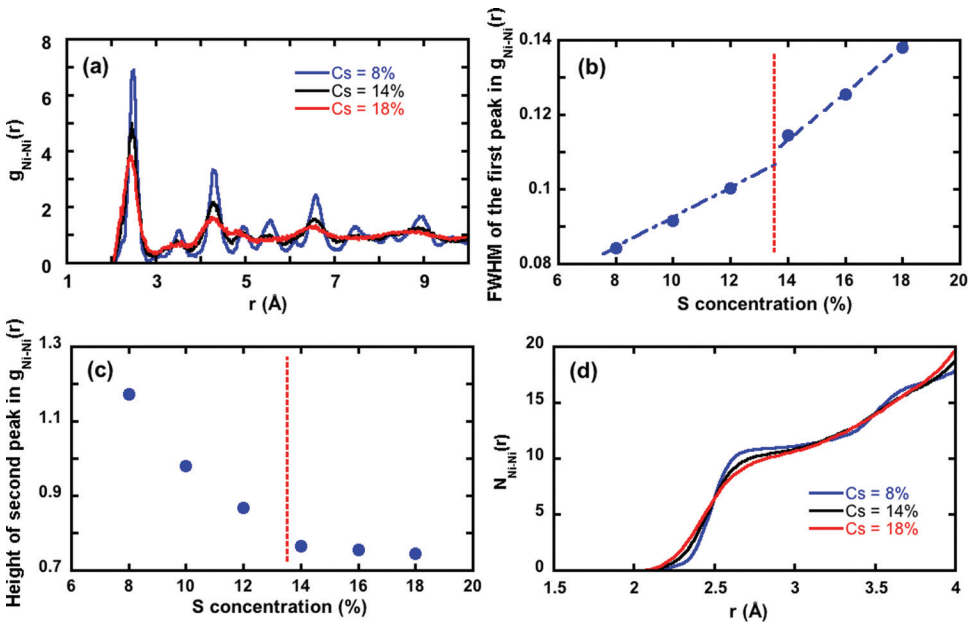


FIG. 1. (Color) (a) Ni-Ni partial pair distribution function $g_{Ni\text{-}Ni}(r)$ of S-doped Ni crystal at different S concentration $c_S$. (b) Full width at half maximum of the first peak of $g_{Ni\text{-}Ni}(r)$ as a function of $c_S$. (c) Height of the second peak of $g_{Ni\text{-}Ni}(r)$ as a function of $c_S$. (d) Coordination number $N_{Ni\text{-}Ni}(r)$ at different S concentration $c_S$.

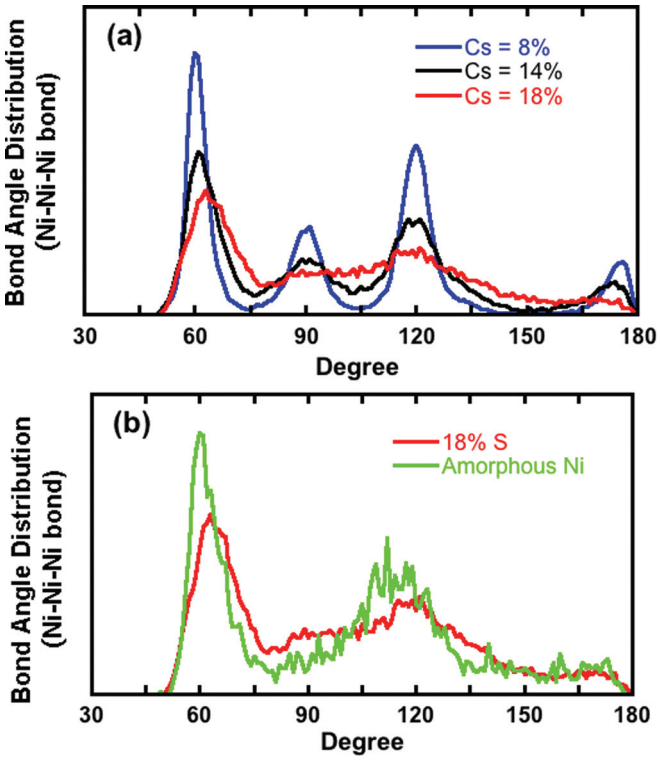


FIG. 2. (Color) (a) Ni-Ni-Ni bond angle distribution (BAD) at S concentrations $c_S = 8$, 14, and 18%. (b) Comparison of the BAD at $c_S = 18\%$ with that of amorphous Ni.

results for the volume expansion relative to the pure Ni crystal, and the dash-dotted and dashed curves, respectively, are the best fits below and above $c_S = 14\%$. Below the critical concentration, the volume is a linear function of the S concentration. In contrast, the volume expansion due to S impurity becomes much greater and nonlinear above 14%, with a visible gap at ~14%, indicating a first-order phase transition.

## III. INTERACTION RANGE OF SULFUR IN NICKEL CRYSTAL AND PERCOLATION ANALYSIS

The structural-correlation analysis in Sec. II reveals a sudden increase of structural disorder in S-doped Ni at a critical S concentration of $c_S \sim 14\%$. It has been speculated that the structural change may be attributed to the steric-size effect of S atoms.[21] The atomic radius of S is known to be much larger than that of Ni,[21] and thus S distorts the Ni fcc lattice, i.e., both Ni-Ni bonds and Ni-Ni-Ni bond angles. Structural phase transition due to such a random substitutional disordering is often described by percolation theory.[22–24] In our system, S impurities in Ni fcc lattice interact through the lattice distortions induced by them. It is thus conceivable that percolation of the lattice distortion-mediated S-S interaction through the entire lattice leads to a global amorphous structure instead of a locally distorted fcc lattice.

In order to apply percolation analysis to the Ni-S system, we need to determine the interaction range between S impurities mediated by lattice distortion. To estimate the S-S interaction range in Ni fcc crystal with S in substitutional sites, we first prepare a Ni crystal containing 5324 atoms ($11 \times 11 \times 11$ unit cells) and calculate the bulk energy $E_{bulk}$ using ReaxFF. Next, we substitute one Ni atom in the crystal with one S atom. The new system is relaxed by ReaxFF-MD, and the final energy $E_1$ of the system is calculated. In this new system, another Ni is substituted with S at a lattice site at distance $d$ from the first S atom, and we calculate the final energy $E_2$ of the system with two S atoms after full relaxation. The calculation procedure is schematically described in Fig. 4, from which the following relations are derived:

$$E_1 = E_{bulk} + E_{1S} + \Delta E_{insert}(S), \tag{2}$$

$$E_2 = E_1 + \varepsilon_{S-S} + E_{1S} + \Delta E_{insert}(S), \tag{3}$$

where $\Delta E_{insert}(S)$ is the energy of inserting one S in Ni crystal, $E_{1S}$ is the energy of an isolated S atom ($=0$ in ReaxFF), and $\varepsilon_{S-S}$ is the interaction energy between two S atoms. Subtracting Eq. (3) from Eq. (2), the interaction energy between two S atoms is obtained from the calculated quantities as

$$\varepsilon_{S-S} = E_2 - 2E_1 + E_{bulk}. \tag{4}$$

Figure 5 shows the calculated interaction energy $\varepsilon_{S-S}$ between two S atoms in the Ni fcc lattice as a function of the S-S distance $d$. $\varepsilon_{S-S}$ takes the minimum value at $d$ equal to the next nearest-neighbor lattice sites, which is close to the lattice constant (LC) = 3.52 Å. Therefore, two S atoms in Ni crystal are most likely to occupy the next nearest-neighbor

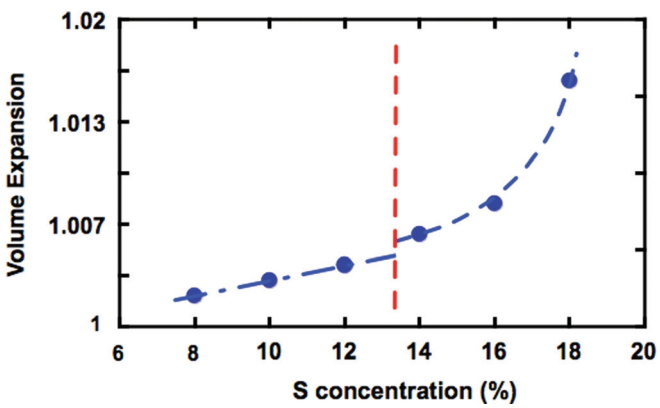


FIG. 3. (Color) Equilibrium volume as a function of S concentration.

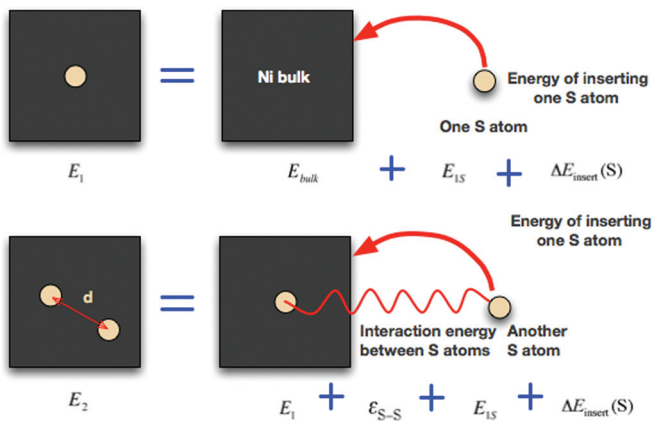


FIG. 4. (Color) Schematic of the calculation procedure for the lattice distortion-mediated S-S interaction energy.

sites. We also see that two S atoms do not have any interaction beyond twice LC, i.e., 7.04 Å.

When the impurity concentration is low, most impurity atoms are likely to stay outside of the interaction ranges of other impurity atoms. As the concentration gets higher, the influence of impurity atoms starts to overlap to form clusters, but the total effect of each cluster is still localized. At a certain critical density, the network of S-S interaction is expected to extend throughout the entire crystal. Such a critical concentration can be calculated based on the percolation theory.[22,23] The site percolation model involves the random occupation (S impurity substitution in our case) of lattice sites of a regular lattice (fcc lattice in our case). Each site of the regular lattice is then randomly occupied with probability $p$. In addition, the model should define the connectivity between the occupied sites. Here, we define two occupied sites within distance $d$ (which is a model parameter) to be connected. The critical occupation probability $p_c$, called percolation threshold, is then defined as the minimum concentration of the occupied sites at which an infinitely connected cluster is formed.[23]

We perform a site percolation simulation to test our hypothesis that the S-induced amorphization of Ni crystal can be explained as a percolation threshold. A system consisting of $100 \times 100 \times 100$ fcc unit cells is simulated with periodic boundary conditions in all three Cartesian directions. In our simulation, lattice sites are randomly occupied with probability $p$. Adjacent sites within the $x$th nearest neighbors ($x = 1$–4, with the corresponding connectivity distance $d = 2.49$–4.98 Å) are defined to be connected to each other, and we enumerate all clusters of such connected sites using a find/union algorithm.[25] Figure 6 shows the largest cluster size (in terms of the number of sites) as a function of the occupation probability $p$ for different connectivity $x$. For each $x$, we observe a critical occupation probability $p_c$, above which the largest cluster size becomes comparable to the total system size. The resulting percolation threshold is 0.20, 0.136, and 0.06, respectively, with the nearest-neighbor (n.n, $x = 1$), next nearest-neighbor (n.n.n, $x = 2$), and the fourth nearest neighbor ($x = 4$) connectivity, in agreement with previous percolation study.[26] Our percolation analysis on fcc lattice thus shows that the critical S concentration for amorphization (0.14) is close to the percolation threshold with the n.n.n connectivity. Note that the n.n.n connectivity is consistent with the most favorable S-S distance due to Ni lattice distortion-mediated interaction as shown in Fig. 5. This serves as a possible explanation of the amorphization transition: For small impurity concentration, the influence of the impurity atoms on structure is localized around each impurity. As the impurity concentration increases, the interaction range of the impurity atoms starts to overlap, and finally becomes global at the percolation threshold to cause amorphization.

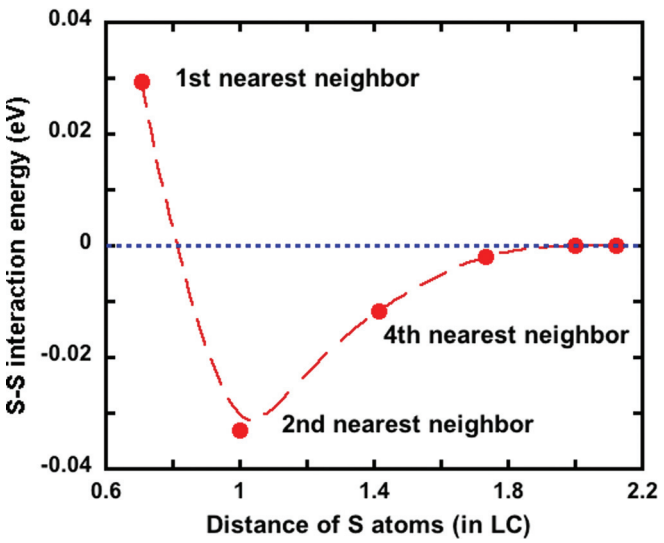


FIG. 5. (Color) S-S interaction energy in Ni fcc crystal as a function of S-S distance (in lattice constant).

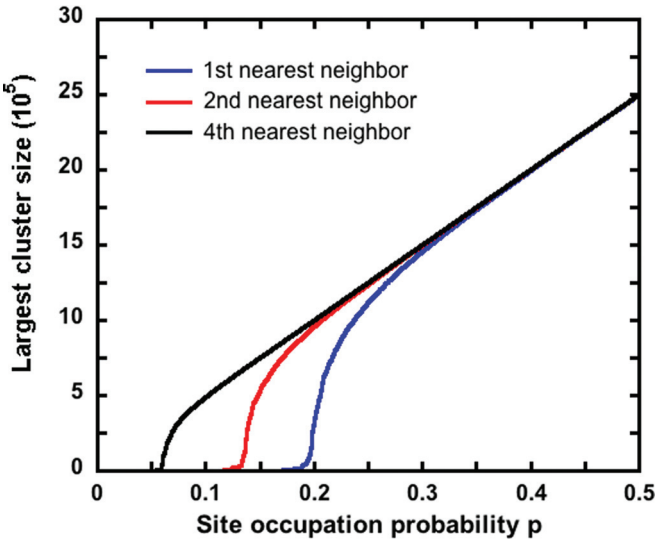


FIG. 6. (Color) The largest cluster size as a function of the occupation probability for fcc lattice considering the 1st, 2nd, and 4th nearest-neighbor connectivity.

## IV. AMORPHIZATION AND PERCOLATION THRESHOLD IN BINARY LENNARD-JONES SYSTEMS

To test the general validity of the amorphization mechanism based on the atomic size effect and percolation of impurity interactions explained in Sec. III, we perform a similar analysis for a binary Lennard-Jones (LJ) system consisting of two types of atoms with different atomic sizes, which has been used extensively to study amorphization. The amorphization of binary systems including binary LJ system has been studied extensively.[27–30] The LJ interatomic potentials are given by

$$\phi_{\alpha\beta}(r_{ij}) = 4\varepsilon\left[\left(\frac{\sigma_{\alpha\beta}}{r_{ij}}\right)^{12} - \left(\frac{\sigma_{\alpha\beta}}{r_{ij}}\right)^{6}\right], \tag{5}$$

where $r_{ij}$ is the interatomic distance between $i$th and $j$th atoms, and $\alpha$ and $\beta$ represent the species of the two atoms (denoted A and B). We define the parameters of the three interactions, $\phi_{AA}$, $\phi_{AB}$ and $\phi_{BB}$ as

$$\varepsilon_{AA} = \varepsilon_{BB} = \varepsilon_{AB} = \varepsilon, \tag{6}$$

$$\sigma_{AB} = (\sigma_{AA} + \sigma_{BB})/2. \tag{7}$$

Thus, all three potentials are taken to be the same depth, and atoms A and B differ only in size.

To find the relationship between the atomic size and interaction range, we use the conjugate-gradient method to perform structural optimization in a similar procedure as we did in determining the S-S interaction range in Sec. III. The system is an fcc lattice consisting of 6912 $(=12\times12\times12\times4)$ atoms. Two B atoms are kept apart at substitutional sites in different distances in the $\langle111\rangle$ direction, and B-B interaction energies are calculated as a function of the distance for different atomic-size ratios, from $\sigma_{AA}/\sigma_{BB}=0.7$ to 0.84.

Figure 7(a) shows the calculated interaction energy as a function of the distance between two B impurity atoms in A crystal with different atomic size ratios $\sigma_{AA}/\sigma_{BB}$. We see that the interaction range varies due to the size effect. For each curve corresponding to a particular atomic size ratio $\sigma_{AA}/\sigma_{BB}$ in Fig. 7(a), we determine the interaction range as the impurity-pair distance at which the interaction energy becomes 0. Figure 7(b) shows the resulting interaction range $R_{int}$ between two impurity atoms as a function of $\sigma_{AA}/\sigma_{BB}$.

Phase diagram in the space of atomic size ratio $\sigma_{BB}/\sigma_{AA}$ and solute concentration $c_S$ for binary LJ solid solution has been obtained by Li *et al.* using MD simulations.[27] Their simulations were performed at a constant pressure and temperature (set to 0 and 0.3, respectively, in reduced LJ units). The corresponding glass transition temperature in LJ liquid is $T_g\sim0.4$. The phase diagram shows the transition from fcc crystal to amorphous structure at increased $c_S$, with different amorphization threshold $c_s^*$ for different atomic size ratio. Figure 7(c) plots $c_s^*$ as a function of $\sigma_{BB}/\sigma_{AA}$.

Figure 7(b) gives the relationship between the atomic size ratio and the impurity interaction range, $R_{int}(\sigma_{AA}/\sigma_{BB})$, which shows a larger interaction range with decreasing $\sigma_{AA}/\sigma_{BB}$. On the other hand, Fig. 7(c) provides the relationship between the atomic size ratio and the amorphization threshold, $c_s^*(\sigma_{AA}/\sigma_{BB})$, which shows a smaller threshold with decreasing $\sigma_{AA}/\sigma_{BB}$. By combining the information—$R_{int}(\sigma_{AA}/\sigma_{BB})$ and $c_s^*(\sigma_{AA}/\sigma_{BB})$—in Figs. 7(b) and 7(c), we can obtain a new mapping between the amorphization threshold and the interaction range, $c_s^*(R_{int})$, as shown in Fig. 8. The figure also shows percolation thresholds obtained by using the 1st, 2nd, and the 4th nearest-neighbor site distances for site connectivity. Namely, the percolation threshold for the fcc lattice considering the 1st, 2nd, and 4th nearest-neighbor connectivity is 0.2, 0.14, and 0.06, respectively, as explained in Sec. III. Figure 8 shows that the crystal-to-amorphous transition in binary LJ system occurs at lower concentrations for larger interaction ranges between impurity atoms. This is consistent with the decreasing percolation threshold as a function of the interaction range in Fig. 8, which supports the conjecture presented in Sec. III, i.e., amorphization occurs at the percolation threshold of the impurity-impurity interaction network.

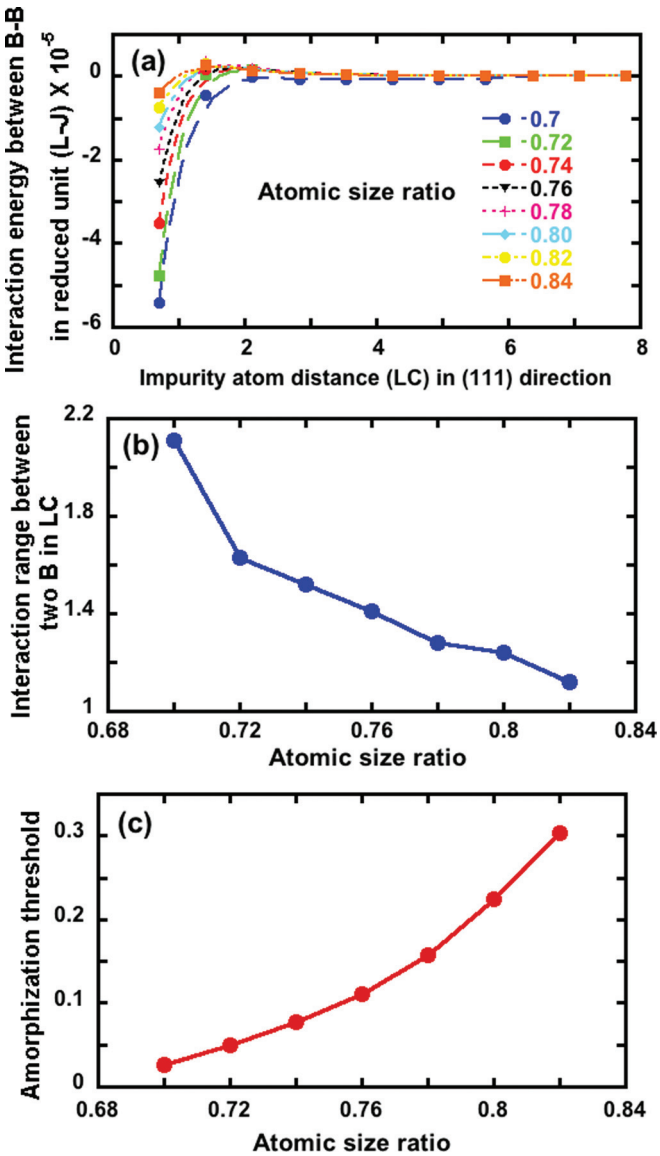


FIG. 7. (Color) (a) Interaction energy vs distance between two B impurity atoms in A crystal in binary Lennard-Jones systems with different atomic size ratios $\sigma_{AA}/\sigma_{BB}$. (b) Interaction range as a function of the atomic size ratio. (c) Amorphization threshold as a function of the atomic size ratio.

## V. SUMMARY

Using reactive force-field molecular dynamics simulations, we have found an atomistic mechanism of sulfur segregation-induced amorphization of nickel. Namely, the

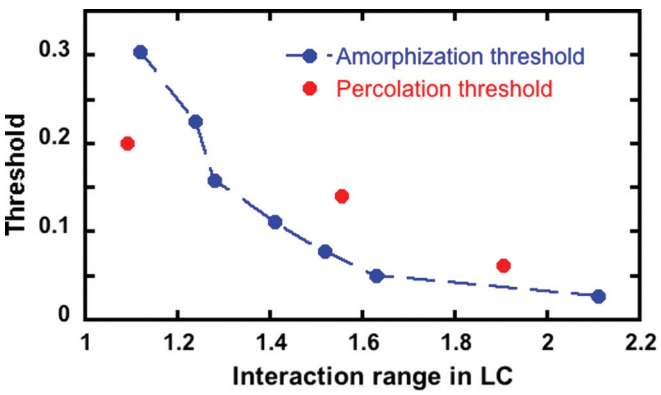


FIG. 8. (Color) Amorphization threshold for binary Lennard-Jones system and percolation threshold as a function of the interaction range (in lattice constant).

large steric size of sulfur impurity causes strong sulfur-sulfur interaction mediated by the distortion of nickel lattice up to the next nearest-neighbor lattice sites, and amorphization occurs at the percolation threshold of the sulfur-sulfur network with the next nearest-neighbor connectivity. The generality of the amorphization mechanism due to the percolation of an impurity network has been confirmed for a binary Lennard-Jones system. Unlike the chemically complex nickel-sulfur system, the binary Lennard-Jones system with a single energy parameter is characterized by only one parameter, i.e., the size ratio between the two types of atoms. The applicability of the proposed percolation-based mechanism for amorphization in such a simple system indicates its applicability to even broader materials.

## ACKNOWLEDGMENTS

This work was supported by DOE-SciDAC/BES. Simulations were performed at the *Argonne Leadership Computing Facility* under the DOE INCITE program and on the 17,280-processor Linux cluster at USC's High Performance Computing Facility.

[1]V. Yamakov, D. Wolf, S. Phillpot, A. Mukherjee, and H. Gleiter, Nature Mater, **1**, 45 (2002).
[2]J. Li, K. Van Vliet, T. Zhu, S. Yip, and S. Suresh, Nature **418**, 307 (2002).
[3]J. Greer, D. Jang, J. Kim, and M. Burek, Adv. Funct. Mater. **19**, 2880 (2009).
[4]D. Farkas, S. Van Petegem, P. Derlet, and H. Van Swygenhoven, Acta Mater. **53**, 3115 (2005).
[5]D. Farkas, S. Mohanty, and J. Monk, Phys. Rev. Lett. **98**, 165502 (2007).
[6]R. P. Messmer and C. L. Briant, Acta Metall. **30**, 457 (1982).
[7]J. Rice and J. Wang, Mater. Sci. Eng. A **107**, 23 (1989).
[8]H. Hofler, R. Averback, H. Hahn, and H. Gleiter, J. Appl. Phys. **74**, 3832 (1993).
[9]C. Koch, J. Mater. Sci. **42**, 1403 (2007).
[10]J. J. Gilman, Science **274**, 65 (1996).
[11]H. C. Rogers, Science **159**, 1057 (1968).
[12]J. K. Heuer, P. R. Okamoto, N. Q. Lam, and J. F. Stubbins, J. Nucl. Mater. **301**, 129 (2002).
[13]T. R. Allen, K. Sridharan, L. Tan, W. E. Windes, J. I. Cole, D. C. Crawford, and G. S. Was, Nucl. Technol. **162**, 342, http://www.new.ans.org/pubs/journals/nt/a_3961 (2008).
[14]H. P. Chen, R. K. Kalia, E. Kaxiras, G. Lu, A. Nakano, K. Nomura, A. C. T. van Duin, P. Vashishta, and Z. Yuan, Phys. Rev. Lett. **104**, 155502 (2010).
[15]A. C. T. van Duin, S. Dasgupta, F. Lorant. and W. A. Goddard, J. Phys. Chem. A **105**, 9396 (2001).
[16]K. Nomura, R. K. Kalia, A. Nakano, and P. Vashishta, Comput. Phys. Commun. **178**, 73 (2008).
[17]K. D. Nielson, A. C. T. van Duin, J. Oxgaard, W. Q. Deng, and W. A. Goddard, J. Phys. Chem. A **109**, 493 (2005).
[18]P. Hohenberg and W. Kohn, Phys. Rev. **136**, B864 (1964).
[19]W. Kohn and P. Vashishta, in *Inhomogeneous Electron Gas*, edited by N. H. March and S. Lundqvist (Plenum, New York, 1983), p. 79.
[20]S. G. Hao, C. Z. Wang, M. J. Kramer, and K. M. Ho, J. Appl. Phys. **107**, 053511 (2010).
[21]M. Yamaguchi, M. Shiga, and H. Kaburaki, Science **307**, 393 (2005).
[22]S. Aharony and A. Aharony, *Introduction to Percolation Theory,* 2nd ed. (Taylor and Francis, London, 1994).
[23]R. Zallen, *The Physics of Amorphous Solids* (Wiley, New York, 1983).
[24]Y. Shi and M. L. Falk, Phys. Rev. B **73**, 214201 (2006).
[25]M. E. J. Newman and R. M. Ziff, Phys. Rev. E **64**, 016706 (2001).
[26]G. Pike and C. Seager, Phys. Rev. B **10**, 1421 (1974).
[27]M. Li and W. L. Johnson, Phys. Rev. Lett. **70**, 1120 (1993).
[28]F. Shimizu, S. Ogata, and J. Li, Acta Mater. **54**, 4293 (2006).
[29]H. Hsieh and S. Yip, Phys. Rev. B **39**, 7476 (1989).
[30]M. Tang and S. Yip, Phys. Rev. Lett. **75**, 2738 (1995).